Proceeding of the IEEE
International Conference on Robotics and Biomimetics
Dali, China, December 2019

Pulse Rate Estimation using PPG Affected with Motion Artifacts Base d on VMD and Hilbert Transform

Wenbo Kang, Min Li, Xinze Che, Jiaxin Wang and Fujun Lai
Department of Mechatronic Engineering and Automation
Shanghai University
Room 421, Mechanical Building,No. 99,Shangda Road, Baoshan District, Shanghai, China
kang93626@ shu.edu.cn & min_li@shu.edu.cn

***Abstract* - Physiological information such as pulse rate (PR) can be extracted from photoplethysmography (PPG) signal. However, pulse rate estimation becomes very difficult during physical exercise since PPG is susceptible to motion artifacts (MA). This paper proposes a PR estimation method using PPG with MA based on variational mode decomposition (VMD) and Hilbert transform. VMD was used to decompose PPG and acceleration signals to generate several intrinsic mode functions (IMFs), respectively. And these obtained IMFs are used to generate corresponding marginal spectrum by Hilbert transform. Finally, MA interference were excluded by spectral peak tracking to obtain accurate PR estimation. The performance of the proposed method has been evaluated using the datasets of 2015 IEEE Signal Processing Cup. Experimental results showed that the average absolute error was 1.97 beat per minute (BPM) and standard deviation of the absolute error was 2.73 BPM. The Pearson correlation between Estimated PR and the ground-truth PR was 0.994. The proposed method can be applied on wearable devices to estimate PR using PPG during physical exercise conditions.**

Index Terms – motion artifacts, variational mode decomposition, Hilbert Transform, pulse rate

I. INTRODUCTION

Photoplethysmography (PPG), as an efficient non-invasive pulse wave detection method, provides a large amount of valuable physiological and pathological information [1-3]. PPG signal are more versatile and wearable than the electrocardiogram (ECG), and it has broad application prospects in detecting physiological information such as pulse rate, blood pressure, respiratory rate and blood oxygen saturation [4-5]. In recent years, pulse rate (PR) monitoring has been widely used in wearable devices such as wristbands and smart watches [6].

However, these devices often have errors in PR estimation, especially during Physical exercise. As a typical medical physiological signal with low frequency characteristics and low signal-to-noise ratio, PPG is very susceptible to noise such as baseline drift, power frequency interference, and motion artifacts (MA) [7]. In particular, MA have the greatest influence on the quality of PPG signal, which seriously affects the correct estimation of PR [8]. MA are mainly caused by lateral or longitudinal displacement between the sensor probe and the skin tissue. The resulting tiny gap increases the interference of [1]ambient light to received signal, and the displacement causes pressure changes in the subcutaneous blood vessels, affecting the ac part of the PPG signal resulting in distortion of the waveform [9].

In practice, the interference of MA causes the real PPG signal to be hidden in the contaminated signal. In the time domain, the PPG waveform is corrupted and periodic features cannot be extracted to estimate PR, in the frequency domain, the frequency range usually generated by MA is above 0.1 HZ, and the PPG signal is a typical low frequency physiological signal whose frequency band is in the range of 0.5-4 HZ. Classical signal processing techniques cannot extract clean PPG from contaminated signals since the frequency bands of MA often overlaps with that of real PPG [10]. Hence, MA elimination in PPG signal is one challenging issue in accurately PR estimation during physical exercise.

Several techniques have been proposed in order to MA removal in PPG signal. The concept of Blind Source Separation (BSS) is the process of separating the clean signal from the aliasing signal where the theoretical model of the signal and the source signal are not accurately detected. The widely used BSS technologies are mainly independent component analysis (ICA) [11], canonical correlation analysis (CCA) [12], principle Component analysis (PCA) [13], and singular spectrum analysis (SSA) [14]. Krishnan et al. [15] proposed using ICA to exclude MA. However, ICA is not suitable for handling contaminated PPG signals because of its statistical independence or irrelevance. Acceleration signal can is a quasi-periodic signal that can be used to exclude MA of the PPG signal. Harishchandra et al. [6] proposed a harmonic sum model for the measuring acceleration and a joint harmonic sum model for the PPG signal destroyed by MA. Zhang et al. [16] proposed the TROIKA framework, including the following core parts: signal decomposition through SSA, signal reconstruction and Spectrum peak tracking. Salehizadeh et al. [17] proposed the SpaMA framework，By comparing the power spectra of PPG and acceleration signals, the frequency peak generated by MA is separated from the PPG power spectrum. Raghuram et al.

* Min Li is the corresponding author.

978-1-7281-6321-5/19//$31.00 ©2019 IEEE

[18] propose an empirical mode decomposition (EMD) method MA elimination based on Hilbert-Huang Transform (HHT).

In this paper, we propose a pulse rate estimation method based on variational mode decomposition (VMD) [19]. The rest part of this paper is as follows. In Section II, we describe the specific implementation of this proposed method. The main steps include PPG and acceleration signals decomposition by VMD, Hilbert transform, spectrum tracking. The performance evaluation and experimental results are shown in Section III. Finally, we have concluded and discussed.

II. METHOD OF PULSE RATE ESTIMATION

The flow chart of the PR estimation method proposed in this paper is shown in Fig. 1. The method is mainly divided into four parts: signal preprocessing, signal decomposition, Hilbert Transform to eliminate MA interference and spectral peak tracking. The original signals used in this paper includes the average signal of two-channel PPG and a three-axis acceleration signal recorded synchronously, and the Ground−Truth heartbeat calculated using the ECG signal is provided along with the data set.

A. Pre-processing

The PR of the human body is 30-240 beats per minute (BPM), which the frequency range is shown as 0.5-4 HZ. In order to adequately retain useful information and remove noises outside the frequency band of interest, such as baseline drift and high-frequency interference, meanwhile, to sparse the spectrum, we preprocessed PPG and acceleration signals by using a band-pass filter to retain signals in the 0.5-4 HZ band before calculation.

Then, the sliding time window size of the PPG and acceleration signals is set to 8 seconds, with a 6 second overlap between each window. This time window size is as same as Zhang et al setting and facilitate the comparison of estimated results with the Ground−Truth heartbeat [16]. Fig.2 shows the original PPG signal after bandpass filtering in a certain time window. Fig. 2(a) indicates that PPG cannot obtain effective features in the time domain since the contamination of MA. Fig. 2(b) shows that there are not only pulse frequencies but also motion frequencies in the spectrum. Correspondingly, Fig. 3 shows the acceleration signal in the same time window. Fig. 3(a) represents the combined acceleration of the three-axis acceleration signal. During the motion process, MA has a certain regularity in a short time, which makes it difficult to extract the pulse rate. Fig. 3(b) shows the severity of the motion disturbance.

The PR estimates calculated by the current window was used as a reference for the next window result. The first time segment has no reference value. Therefore, try to ensure that the signal is in a stable state at the beginning of the signal, use the spectrum of the acceleration to exclude the MA interference, and then select the frequency with the largest amplitude to calculate the initial pulse rate.

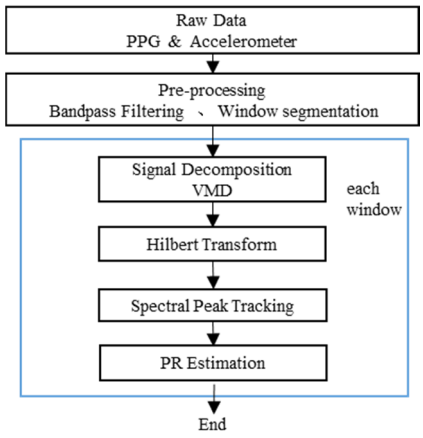

Fig. 1 The flow chart of the PR estimation

A. Signal Decomposition

Konstantin et al. [19] proposed a variable scale signal decomposition algorithm VMD, which has been widely applied. VMD is a signal decomposition algorithm for non-stationary signals and an improvement of EMD algorithm. Compared with EMD, VMD can better avoid the problem of modal aliasing and endpoint effects [20]. It has been applied in the field of fault diagnosis, medical signal processing, etc.

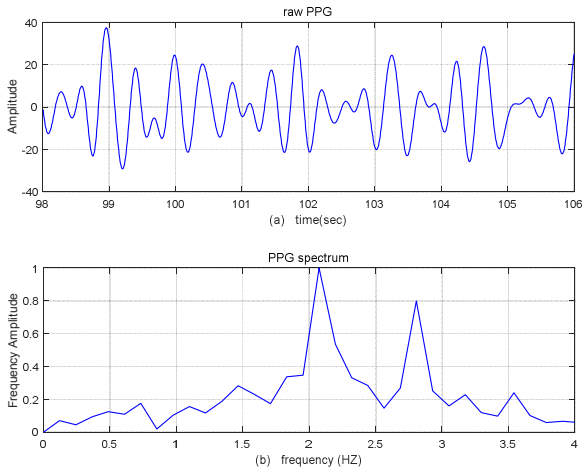

Fig. 2 Raw PPG Signal in one time window

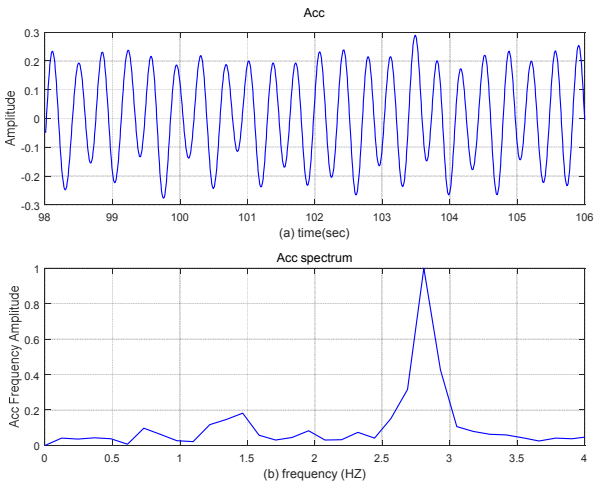

Fig. 3 Accelerometer Signal in one time window

VMD method is used to decompose the original signals into k intrinsic mode functions (IMFs), where k is the preset decomposition scale.

In the VMD algorithm, the IMFs $u_n(t)$ is redefined as an amplitude modulated signal, as shown in Eq. (1).

$$u_n(t) = A_n(t)\cos\left(\omega_n(t)\right) \tag{1}$$

where $u_n(t)$ is the n-th IMF，$A_n(t)$ is the instantaneous amplitude of $u_n(t)$，$\omega_n(t)$ is instantaneous frequency of $u_n(t)$, $\omega_n(t) = \varphi_k(t) = \frac{d\varphi(t)}{dt}$.

Each component is concentrated at the center frequency ω_n, and the Gaussian smoothed offset signal can be used to estimate the bandwidth. Due to the sparsity of the VMD, it can be converted into the following problem during decomposition.

$$\min_{\{u_n\}\{\omega_n\}} \left\{ \sum_n \left\| \partial_t \left[\left(\sigma(t) + \frac{j}{\pi t} \right) u_n(t) \right] e^{i-j\omega_n t} \right\|_2^2 \right\} \tag{2}$$

$$\sum_{n=1}^{N} u_n = x(t) \tag{3}$$

where $u_i = [u_1, u_2, \ldots, u_n]$ means k-th intrinsic mode function，$\omega_i = [\omega_1, \omega_2, \ldots, \omega_i]$ is center frequency of u_i.

Introducing the Lagrangian multiplier λ and the second penalty α to convert the above problem into unconstrained and variational, as shown in Eq. 4.

$$\begin{aligned} L(\{u_k\}\{\omega_k\}\{\lambda\}) = \alpha \sum_n \Big\| \partial_t \Big[\Big(\sigma(t) \\ + \frac{j}{\pi t} \Big) u_n(t) \Big] e^{i-j\omega_n t} \Big\|_2^2 \\ + \Big\| \mathrm{x(t)} - \sum_n u_n(t) \Big\|_2^2 \\ + \langle \lambda(t), x(t) - \sum_n u_n(t) \rangle \end{aligned} \tag{4}$$

where α represents quadratic penalty term and λ represents Lagrangian multiplier.

VMD assumes that each IMF u_i is a finite bandwidth around the center frequency, and adaptively decomposes the signal by looking for the optimum solution of the constrained variational model. The optimum solution of the variational model is iteratively obtained from the center frequency and bandwidth of each IMF. The original signal is adaptively decomposed according to the continuous updating of the frequency domain features. The actual signal is decomposed into several IMFs.

The main parameters of the VMD algorithm include: α (quadratic penalty term), K (number of resolved IMFs), τ (fidelity coefficient), and e (discriminant precision). The study found that the τ and e have little effect on the decomposition effect, and the default value in VMD is usually adopted, and parameters α and K have a great influence on the decomposition effect. The choice of α affects the accuracy of the decomposition. If the value is too low, the decomposition result will be inaccurate. If the value is too high, the calculation time of the decomposition will increase, and even the program will be infinite loop.

VMD demands to preset the quantity of decomposed IMFs to K. Inappropriate K value may bring a large error to the decomposition result. If K is less than the number of real component (under-decomposition), it means that the number of IMFs after decomposition is smaller than the actual component, and the result of the decomposition may cause modal aliasing [21]. If K is much larger than the number of real components, the decomposition result may be distorted, and the variable without actual physical meaning is decomposed.

In this paper, we have experimentally set the alpha value to 2000, which improves the decomposition efficiency while ensuring the decomposition accuracy. Singular value decomposition (SVD) [22] is used to determine the number K of IMFs. The PPG signal is subjected to singular value decomposition to obtain a set of singular values σ, which can reflect the concentration of signal and noise energy. The first K large singular values concentrate most of the energy. We use the K value determined by SVD to determine the IMFs number of VMD.

After determining the parameters of the VMD, we decompose the PPG signal and the combined acceleration signal to obtain IMFs. Taking Figure 4 as an example, SVD for PPG generates a singular value vector that most of the amplitude distribution is in the first 6 vector values. Therefore, the parameter value K of the VMD is set to 6, the PPG is decomposed into 6 IMFs, and the graph on the right represents the spectrum obtained using FFT of imf1 to imf6, respectively. Some of IMF which have a dominant peak can be further processed to estimate pulse rate.

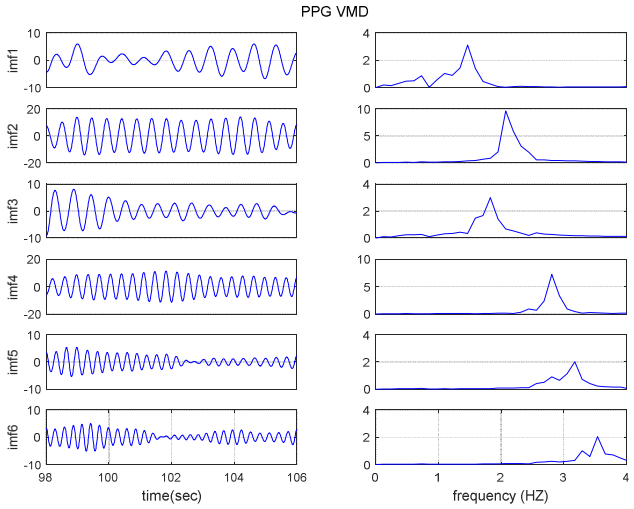

Fig. 4 PPG performs VMD to get IMFs

The clean PPG and MA components are contained in different IMFs ($imf_1, \ldots, imf_k$). According to the corresponding frequency of acceleration IMFs we can remove the MA signal to get the clean PPG signal.

B. Hilbert Transform

After VMD, the PPG and acceleration signals are adaptively decomposed into a finite quantity of IMFs. In order to better describe the change of frequency with time, time-frequency analysis is performed on the IMFs by Hilbert transform.

Norden E Huang proposed the Hilbert-Huang transform (HHT) [23]. The signal is decomposed into a finite quantity of IMFs by EMD and subjected to a Hilbert transform. In this paper, VMD is utilized for signal decomposition.

Each IMF obtained by decomposition is subjected to spectral analysis by Hilbert transform, and the instantaneous frequency of the signal as shown in Eq. (5)

$$x(t) = Re\left[\sum_{j=1}^{n} a_j(t)\ e^{i\theta_j(t)}\right] = Re\left[\sum_{j=1}^{n} a_j(t)\ e^{i\int \omega_j(t)dt}\right] \quad (5)$$

where Re represents the real part, $\theta_j(t)$ represents the argument of the polar form of the analytical signal formed by Hilbert Transform for each IMF, and $\omega_j(t)$ is the instantaneous frequency of each IMF. The right part of the Eq. (5) is the Hilbert time-frequency spectrum, which is recorded as:

$$H(\omega, t) = Re\left[\sum_{j=1}^{n} a_j(t)\ e^{i\int \omega_j(t)dt}\right] \quad (6)$$

Then the marginal spectrum is defined as:

$$H(\omega) = \int_{-\infty}^{\infty} H(\omega, t)\, dt \quad (7)$$

Compared with the commonly used power spectrum, the marginal spectrum can significantly improve the local characteristic response accuracy and resolution of the signal, and can effectively suppress energy leakage. In consideration of the above advantages of the marginal spectrum, the marginal spectrum is used for pulse rate frequency detection. PPG and acceleration marginal spectrum are shown in Fig. 5.

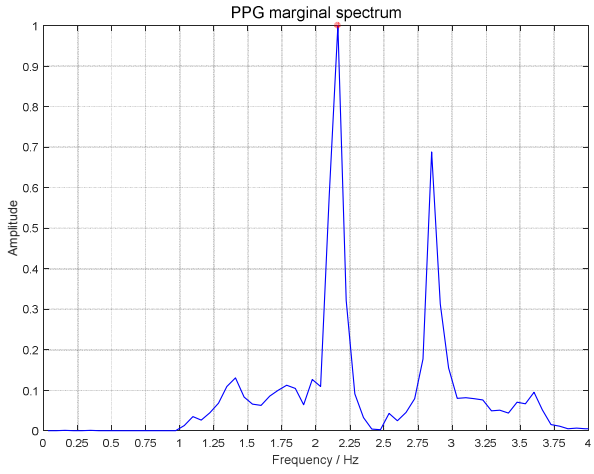

(a) PPG marginal spectrum

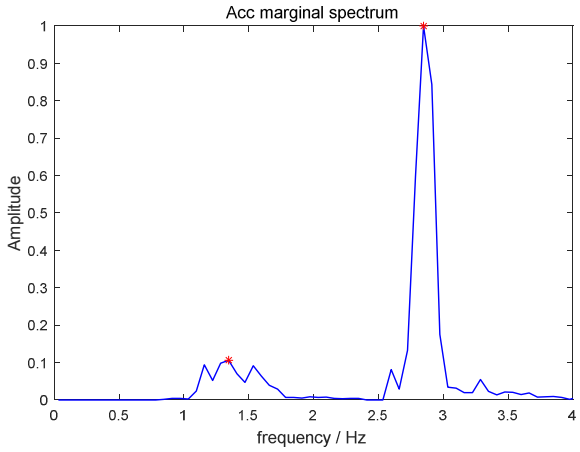

(b) acceleration marginal spectrum

Fig. 5 PPG and acceleration marginal spectrum

C. *Spectral Peak Tracking*

In this step, the function is to exclude the interference of MA in the spectrum to identify the frequency of the pulse rate. In the acceleration marginal spectrum, the motion dominant frequency can be obtained by extracting the frequency peak. Spectral peaks with amplitude greater than 20% (marginal spectrum has been normalized to the range of 0-1) were extracted as the dominant frequency of motion and stored in vector M, which is expressed as

$$M = [m_1, m_2, \dots, m_k] \quad (8)$$

In the PPG marginal spectrum, the peaks (magnitude greater than 20%) that are likely to represent the PR are also selected and stored in the candidate frequency vector H, which is denoted as

$$H = [h_1, h_2, \dots, h_n] \quad (9)$$

$h_i (h_i \subset H)$ may represent the frequency of pulse rate or MA interference. When h_i is equal or very close to $m_j (m_j \subset M)$, the frequency to be selected h_i can be considered as a motion frequency, and this frequency can be deleted from the vector H to get H'.

Then select h_i' from H' and compare it with the prior information PR_{pre}. PR_{pre} is the PR calculated from the previous window. There is a 6 second overlap between adjacent time windows. If the two adjacent time windows overlap too much, the calculated PR values are very close. PR does not change drastically in a short time, so the value calculated in the previous window can be used as reference information for the current window. Similarly, the PR calculated by the current window needs to be the prior information of the next window. If the calculated PR of h_i' is more than 10 BPM different from PR_{pre}, this h_i' is deleted and H'' is obtained.

H'' was obtained by deleting several interference frequencies, and two situations may occur. In one case, there is still exist frequencies to be selected in H'', and the candidate frequency with the largest peak amplitude is selected as the simulated PR frequency of the time window, and as the

reference PR of the next time window. The current estimated PR is expressed as

$$\mathrm{PR}_{cur} = 60 * {h_i}'_{max} \tag{10}$$

In another case, H'' is null, indicating that the PR frequency peak is submerged in the MA noise in the marginal spectrum under strong motion interference, and the frequency characteristics cannot be extracted. We choose to use the Fourier spectrum as the auxiliary information for frequency searching. The spectrum is obtained by Fourier transform from the IMF obtained by PPG decomposition, and the candidate frequency vector F（$\{f_{s1}, f_{s2}, \ldots, f_{sn}\}$） is obtained according to the above steps. Then, according to the acceleration frequency, the frequency dominated by the MA is removed, and the frequency $f_{si_{closest}}$ to be selected closest to the PR_{pre} frequency is selected as the PR frequency of the time window. The current estimated PR is expressed as

$$\mathrm{PR}_{cur} = 60 * f_{si_{closest}} \tag{11}$$

If $f_{si_{closest}}$ is null, represents there is still no candidate frequency in F to satisfy the condition, we select PR_{pre} as the PR of this window. The current estimated PR is expressed as

$$\mathrm{PR}_{cur} = \mathrm{PR}_{pre} \tag{12}$$

III. Experimental Results

A. Data Sources

The data set used in this paper has been collected and published by Zhang et al. [16]. All data used include two-channel PPG signals, three-axis accelerometer signals and one-channel ECG signal. For each subject, the pulse signal at the wrist was recorded by two green light (wavelength of 515nm) source PPG sensors at a distance of 2 cm. The three-axis accelerometer records the acceleration signal synchronously on the wrist. The PPG sensors and accelerometer are fixed in the wristband worn by the subject. The ECG signal was recorded simultaneously from the chest using wet ECG sensors. The ground-truth PR is calculated by ECG. The sampling rate of all signals is set to 125HZ. Each subject ran on a treadmill with dynamic speeds during data recording.

B. Performance Measurement

To evaluate the performance of the PR estimation method proposed in this paper, several indicators were used. The average Absolute Error (AE_{avg}) is defined as

$$AE_{avg} = \frac{1}{N}\sum_{i=1}^{N}|PR_i - BPM_i| \tag{13}$$

where N represents the total number of time windows, PR_i and BPM_i represent the estimated and true PR value in current time , respectively. Standard Deviation of the Absolute Error (AE_{sd}) and Average Relative Error (RA_{avg}) were defined as

$$AE_{sd} = \sqrt{\frac{1}{N}\sum_{i=1}^{N}(PR_i - BPM_i)^2} \tag{14}$$

$$RA_{avg} = \frac{1}{N}\sum_{i=1}^{N}\frac{|PR_i - BPM_i|}{BPM_i} \tag{15}$$

The consistency between BPM_i and PR_i, is represented by Bland-Altman diagram, which indicates the difference between each estimated PR and the actual PR with respect to the average value. Pearson correlation between estimated PR and the actual PR was also assessed.

C. Results

The proposed method shows that the AE_{avg} was 1.97 BPM, AE_{sd} was 2.73 BPM and RA_{avg} was 1.48%. The experimental results of each subjects are shown in Table I, and the performance of the proposed method has a certain improvement compared with TROIKA[16]. Fig.6 and Fig.7 illustrate the Bland-Altman and the Person coefficient diagram, respectively. In order to visually display the effect of PR estimation，Fig.8 shows the estimate result from the subject No.9. It is obvious that this proposed method has good performance for dynamic pulse rate estimation during physical exercise.

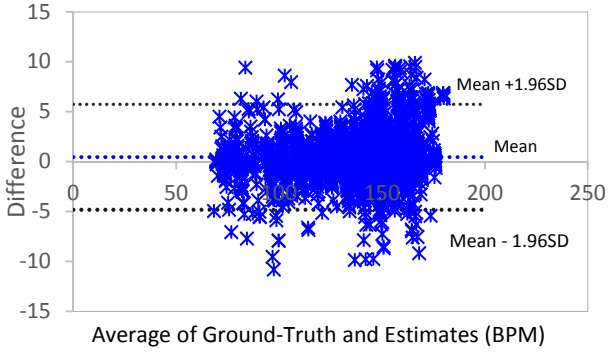

Fig. 6 The Bland-Altman plot

TABLE I
THE AVERAGE ABSOLUTE ERROR (BPM) AND AVERAGE RELATIVE ERROR OF 12 SUBJECTS USING THIS PROPOSED METHOD AND TROIKA

		1st	2nd	3rd	4th	5th	6th
AE_{avg}	Proposed method	2.76	1.57	1.35	1.94	1.88	2.28
	TROIKA	2.29	2.19	2.00	2.15	2.01	2.76
RA_{avg} (%)	Proposed method	2.19	1.34	1.10	1.67	1.38	1.83
	TROIKA	1.90	1.87	1.66	1.82	1.49	2.25
		7th	**8th**	**9th**	**10th**	**11th**	**12th**
AE_{avg}	Proposed method	1.71	1.80	1.49	2.64	2.85	2.64
	TROIKA	1.67	1.93	1.86	4.70	1.72	2.84
RA_{avg} (%)	Proposed method	1.28	1.45	1.19	1.67	1.86	2.10
	TROIKA	1.26	1.62	1.59	2.93	1.15	1.99

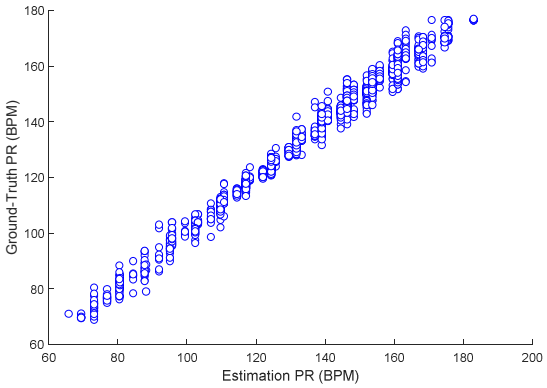

Fig. 7 Pearson correlation of the estimation and Ground-Truth of PR

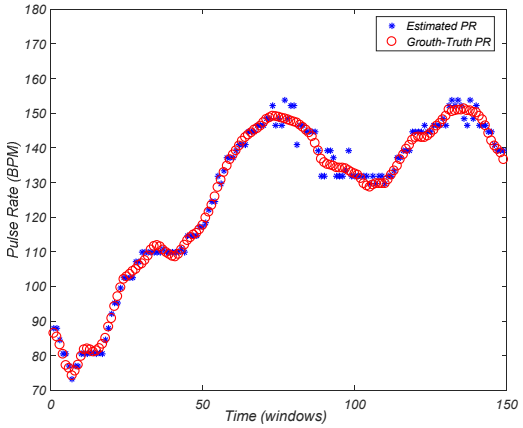

Fig. 8 The PR estimation result from subject 9

IV. CONCLUTIONS

In this paper, we propose a dynamic pulse rate estimation method using PPG and acceleration signal during physical exercise, where VMD and Hilbert transform were applied to eliminate interference from MA. Experiments show that VMD is suitable for decomposing medical non-stationary signals similar to PPG, and does not produce modal aliasing problems. A good estimate of the pulse rate were obtained using PPG and acceleration signals obtained from the wrist. This proposed method has good feasibility on wearable devices.

In addition, a method of determining the mode decomposition number based on the singular value energy distribution of the SVD algorithm is used. A feasible scheme is proposed to determine the number of mode decompositions of the VMD algorithm.

REFERENCES

[1] Yadav U, Abbas S N, Hatzinakos D. Evaluation of PPG biometrics for authentication in different states[C]//2018 International Conference on Biometrics (ICB). IEEE, 2018: 277-282.

[2] Thomas S S, Nathan V, Zong C, et al. BioWatch: A noninvasive wrist-based blood pressure monitor that incorporates training techniques for posture and subject variability[J]. IEEE journal of biomedical and health informatics, 2015, 20(5): 1291-1300.

[3] Moraes J, Rocha M, Vasconcelos G, et al. Advances in photopletysmography signal analysis for biomedical applications[J]. Sensors, 2018, 18(6): 1894.

[4] Xu Y, Ping P, Wang D, et al. Analysis for the Influence of ABR Sensitivity on PTT-Based Cuff-Less Blood Pressure Estimation before and after Exercise[J]. Journal of healthcare engineering, 2018.

[5] Jarchi D, Charlton P, Pimentel M, et al. Estimation of respiratory rate from motion contaminated photoplethysmography signals incorporating accelerometry[J]. Healthcare technology letters, 2019, 6(1): 19-26.

[6] Dubey H, Kumaresan R, Mankodiya K. Harmonic sum-based method for heart rate estimation using PPG signals affected with motion artifacts[J]. Journal of Ambient Intelligence and Humanized Computing, 2018, 9(1): 137-150.

[7] Temko A. Accurate heart rate monitoring during physical exercises using PPG[J]. IEEE Transactions on Biomedical Engineering, 2017, 64(9): 2016-2024.

[8] Islam M S, Shifat-E-Rabbi M, Dobaie A M A, et al. PREHEAT: Precision heart rate monitoring from intense motion artifact corrupted PPG signals using constrained RLS and wavelets[J]. Biomedical Signal Processing and Control, 2017, 38: 212-223.

[9] Ghairat J, Mouhsen H. Motion artifact reduction in PPG signals[J]. 2015.

[10] Harvey J, Salehizadeh S M A, Mendelson Y, et al. OxiMA: A Frequency-Domain Approach to Address Motion Artifacts in Photoplethysmograms for Improved Estimation of Arterial Oxygen Saturation and Pulse Rate[J]. IEEE Transactions on Biomedical Engineering, 2018, 66(2): 311-318.

[11] Hyvärinen A, Oja E. Independent component analysis: algorithms and applications[J]. Neural networks, 2000, 13(4-5): 411-430.

[12] Thompson B. Canonical correlation analysis: Uses and interpretation[M]. Sage, 1984.

[13] Jolliffe I. Principal component analysis[M]. Springer Berlin Heidelberg, 2011.

[14] Elsner J B, Tsonis A A. Singular spectrum analysis: a new tool in time series analysis[M]. Springer Science & Business Media, 2013.

[15] Krishnan R, Natarajan B, Warren S. Two-stage approach for detection and reduction of motion artifacts in photoplethysmographic data[J]. IEEE transactions on biomedical engineering, 2010, 57(8): 1867-1876.

[16] Zhang Z, Pi Z, Liu B. TROIKA: A general framework for heart rate monitoring using wrist-type photoplethysmographic signals during intensive physical exercise[J]. IEEE Transactions on biomedical engineering, 2014, 62(2): 522-531.

[17] Salehizadeh S, Dao D, Bolkhovsky J, et al. A novel time-varying spectral filtering algorithm for reconstruction of motion artifact corrupted heart rate signals during intense physical activities using a wearable photoplethysmogram sensor[J]. Sensors, 2015, 16(1): 10.

[18] Raghuram M, Madhav K V, Krishna E H, et al. HHT based signal decomposition for reduction of motion artifacts in photoplethysmographic signals[C]//2012 IEEE International Instrumentation and Measurement Technology Conference Proceedings. IEEE, 2012: 1730-1734.

[19] Dragomiretskiy K, Zosso D. Variational mode decomposition[J]. IEEE transactions on signal processing, 2013, 62(3): 531-544.

[20] Nazari M, Sakhaei S M. An efficient method for extracting respiratory activity from single-lead-ECG based on variational mode decomposition[C]//2015 22nd Iranian Conference on Biomedical Engineering (ICBME). IEEE, 2015: 194-198.

[21] Sharma H. Heart rate extraction from PPG signals using variational mode decomposition[J]. Biocybernetics and Biomedical Engineering, 2019, 39(1): 75-86.

[22] Wall M E, Rechtsteiner A, Rocha L M. Singular value decomposition and principal component analysis[M]//A practical approach to microarray data analysis. Springer, Boston, MA, 2003: 91-109.

[23] Wang Q, Yang P, Zhang Y. Artifact reduction based on Empirical Mode Decomposition (EMD) in photoplethysmography for pulse rate detection[C]//2010 Annual International Conference of the IEEE Engineering in Medicine and Biology. IEEE, 2010: 959-962.